Bioelectrochemistry 74 (2008) 101–110

Contents lists available at ScienceDirect

Bioelectrochemistry

journal homepage: www.elsevier.com/locate/bioelechem

# Surface characterization and direct electrochemistry of redox copper centers of bilirubin oxidase from fungi *Myrothecium verrucaria*

Dmitri Ivnitski *, Kateryna Artyushkova, Plamen Atanassov *

*Chemical and Nuclear Engineering Department, University of New Mexico, Albuquerque, NM 87131, USA*

ARTICLE INFO

*Article history:*
Received 20 March 2008
Received in revised form 5 May 2008
Accepted 8 May 2008
Available online 19 May 2008

*Keywords:*
Bilirubin oxidase
Fungus *Myrothecium verrucaria*
Redox potentials of T1 and T2/T3 copper centers
Direct electron transfer
Angle-resolved XPS

ABSTRACT

The key characteristics of multicopper oxidases are redox potentials of Type 1, Type 2 and Type 3 copper centers of enzymes. However, there is still a challenge to obtain a value of the redox "signature" of the enzymes. In this study, the electrochemical behavior of T1 and T2/T3 redox copper centers of bilirubin oxidase (BOD) from the fungi *Myrothecium verrucaria* was studied based on direct bioelectrocatalysis. Two distinct redox peaks corresponding to reduction and oxidation of T1 and T2/T3 redox centers of enzymes have been clearly detected in anaerobic conditions. The bioelectrocatalytic activity of the enzyme was studied in the presence of oxygen and redox mediators. The electron-transfer rate constant for BOD immobilized on carbon electrode (CE) is 1.5 $s^{-1}$. The mechanism of enzyme inactivation by ABTS has been proposed. The physical architecture of BOD layers immobilized on the electrode surface, including elemental and chemical composition, relative thickness and assembly of layers was investigated by Angle Resolved X-ray photoelectron spectroscopy. Unique peaks of BOD at 288.5 eV and of CE at 284.6 eV were used in a substrate over layer model for estimation of the thickness of the of BOD film on the carbon electrode surface.
Published by Elsevier B.V.

## 1. Introduction

Direct electrical communication between redox centers of an enzyme and an electrode is a subject of interest for studying the kinetics and the mechanism of biological redox processes as well as for practical applications of bioelectrochemistry in the design and development of microscale electrochemical biosensors, biomedical devices, and biofuel cells [1–10]. For efficient operation of enzyme-based biofuel cells a number of conditions must be satisfied. First, the enzymes should have high catalytic activity, stability, and be inexpensive. Second, the process of bioelectrocatalysis requires developing methodology of mediation and enzyme immobilization for efficient electron transfer from the enzyme to the electrode surface. Third, the open circuit potential of the enzyme electrode must be close to the redox potential of enzymes itself to give the maximum potential difference between the anode and cathode. In this respect, the most attractive enzymes for biofuel cell application are glucose oxidase for bioanode and bilirubin oxidase or laccase for biocathode development [6–10].

The bilirubin oxidase (BOD) from *Myrothecium verrucaria* is a monomeric enzyme with molecular mass of 66 kDa [11,12]. It has a negative charge in neutral solution; the isoelectric point of the enzyme is 4.2 [13]. The active site of BOD consists of four copper ions classified into Type 1 (T1), Type 2 (T2), and Type 3 (T3). The T1 copper is connected to the trinuclear T2/T3 copper center by a His–Cys–His tripeptide [11]. Type 1 provides long range intramolecular electron transfer from electron-donating substrates to the trinuclear copper center. The T2/T3 copper center plays a key role in the oxygen reduction to water. BOD can operate at pH 5 and at neutral pH and is not inhibited by chloride ions [14–16]. In addition to its native substrate, bilirubin oxidase is able to oxidize organic and inorganic substrates while catalyzing oxygen reduction to water. The reaction mechanism of BOD has been studied intensively by spectroscopic methods, such as EPR, magnetic circular dichroism and X-ray absorption spectroscopy [11,12,17,18].

The key characteristics of BOD are the redox potentials of T1 and T2/T3 copper centers of the enzyme [12,14–16,19,20–24]. The formal redox potential of T1 was found to be 260 mV vs. Ag/AgCl at pH 5.3 [19], but other studies reported more positive potentials >400 mV vs. Ag/AgCl at pH 7 [12,14–16,20–22,24]. The half-wave potential of oxygen reduction at pH 7.4 was found to be +0.605 V vs. NHE [14]. Under anaerobic conditions, cyclic voltammograms obtained with BOD-modified carbon electrodes did not show anodic and cathodic peak currents related to the T2/T3 redox copper center of BOD [14,24,25]. Recently, two ET processes, in the low and in the high potential, 400 and 670 mV vs. NHE, respectively, were seen for BOD from *M. verrucaria* at gold electrodes [22]. However, it is still a challenge to determine the redox potential for T2/T3 redox center by using conventional potentiometric-spectroscopic titration as a result

* Corresponding authors. Ivnitski is to be contacted at University of New Mexico, Department of Chemical and Nuclear Engineering, MSC01 1120, 209 Farris Engineering Center, Albuquerque, NM 87131-0001, USA. Tel.: +1 505 277 7952. Atanassov, Tel.: +1 505 277 2640; fax: +1 505 277 5433.
*E-mail addresses:* ivnitski@unm.edu (D. Ivnitski), plamen@unm.edu (P. Atanassov).

1567-5394/$ – see front matter. Published by Elsevier B.V.
doi:10.1016/j.bioelechem.2008.05.003

of spectral overlap between mediators and proteins [26–28]. Measuring redox states of BOD in anaerobic conditions is impossible because the intermediate redox states are formed during the catalytic turnover of the enzyme in the presence of oxygen only. The absorbance of many mediators used for redox titration of the enzyme coincides with the absorbance changes of the T2/T3 center during its redox transformation [18]. The complexity of multicopper redox enzymes has made it difficult to fully understand the various electron-transfer events. Therefore, the precise mechanism of enzymatic dioxygen reduction is still not fully clarified.

The focus of this research is studying the electrochemical behavior of BOD from *M. verrucaria*. Here we attempted to determine redox potentials of both T1 and T2/T3 redox copper centers and to understand the mechanism of intramolecular electron transfer which occurs within BOD. The electrochemical behavior of BOD has been studied by using the Protein Film Voltammetry (PFV) approach. The concept and theory of PFV was described comprehensively [29–33]. Since the redox centers of BOD are located deep within the protein, direct heterogeneous electron transfer between the redox centers of enzyme and the electrode is a challenge. Recently numerous efforts have been made to reduce the electron tunneling distance by using different promoters: layered polyion-protein films [34–36], redox relay applications [6,16,37], and self-assembled monolayers [38–40]. Significant breakthrough in this area of research has been achieved by using carbon nanotubes (CNTs) and other electroconductive nanoparticles as promoters of direct bioelectrocatalysis [8,41–45]. In this paper, to create ultrathin nanometer range BOD films we have used two approaches: (1) layer-by-layer deposition and (2) co-immobilization of BOD and carbon nanotubes followed by their encapsulation into a Nafion film. Both approaches facilitate direct electron transfer (DET) between redox centers of BOD and the carbon electrode. The layer-by-layer technique provides a simple, fast, and reproducible method of enzyme immobilization under mild conditions [34–36]. The single-walled carbon nanotubes, which have a small size, excellent chemical stability and a range of electrical conductivity [41–45], have been used as conducting nanowires for DET between the redox centers of BOD and the electrode surface. Fig. 1 presents a principle schematic of the mechanistic aspects of DET electro-reduction of molecular oxygen catalyzed by BOD in contact with CNT (Fig. 1a). The physical architecture of ultra thin BOD films, including elemental and chemical composition, relative thickness and assembly of layers, have been investigated in detail by Angle Resolved X-ray photoelectron spectroscopy (ARXPS). ARXPS is a powerful technique allowing estimation of the elemental and chemical composition of the upper 10 nm of a surface and has been demonstrated to be an effective tool to quantify protein immobilized or adsorbed during enzyme immobilization [46]. The ARXPS has several advantages, including surface sensitivity, a non-destructive nature, and the ability to provide both elemental and chemical information [47]. It has been widely used to study different types of multi layered systems such as Langmuir Blodgett films and self-assembled monolayers [48].

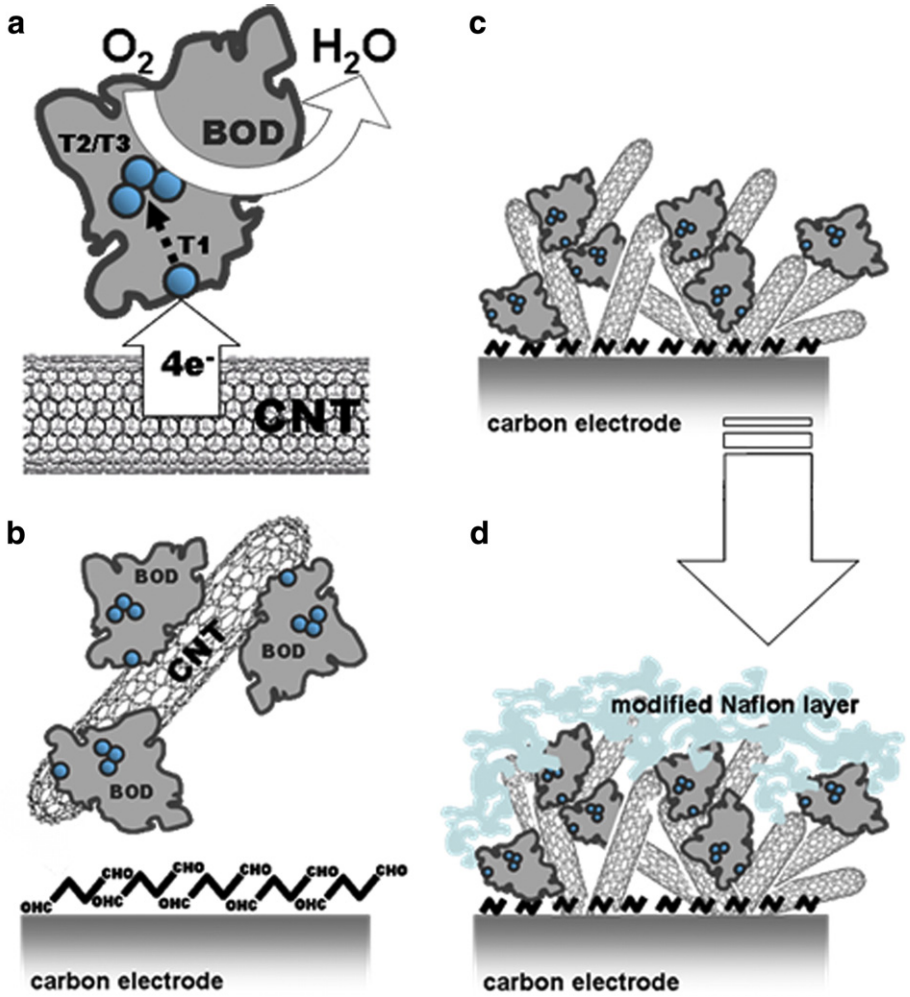


**Fig. 1.** Schematic illustration of a direct electrical communication between redox centers of bilirubin oxidase and CNT modified electrode. The Nafion membrane acts as a binder to hold the BOD/CNT on the electrode surface.

## 2. Experimental

### 2.1. Reagents

Bilirubin oxidase (BOD) from *M. verrucaria*, bilirubin, 2,2-azino-bis (3-ethylbenzothiazoline-6-sulfonic acid) (ABTS), single-walled carbon nanotubes (SWNTs), hydroquinone (HQ), bathocuproine disulfonate, glutaraldehyde (GA), and polyethilenimine (PEI) were obtained from Sigma (St. Louis, MO). Tetrabutylammonium bromide salt-treated Nafion® was obtained from Professor Shelley Minteer from Saint Louis University [64]. Other chemicals of analytical grade were obtained from standard sources. All solutions were prepared with deionized water.

### 2.2. Methods of BOD immobilization on a carbon electrode surface

#### 2.2.1. Layer-by-layer approach

A multilayer architecture, which contains ordered layers of BOD, was assembled by means of alternate electrostatic adsorption with positively charged poly(ethylenimine) (PEI). The pH of the buffer solution was set far apart from the isoelectric point of BOD so that the enzyme was sufficiently negatively charged under the experimental conditions. The first BOD/PEI layer was prepared similar as reported for laccase electrode preparation [49]. Prior to coating, the surface of a cleaned working carbon electrode was activated by 10% glutaraldehyde for 1 h. The adsorbed glutaraldehyde molecules were used for creating a stable first monolayer of BOD molecules by their lateral cross-linking. After extensive washing and drying of the glutaraldehyde modified carbon surface, 10 µl of the BOD solution (10 mg/ml) were applied to the surface of carbon working electrode, and the electrode was incubated for 45 min at room temperature. To remove unbound enzyme, the working electrode was washed three times with phosphate buffer (pH 7.0). Then 10 µl of 0.1% PEI solution were applied to the electrode surface for 45 min and the electrode was washed three times with phosphate buffer. The PEI forms a positively charged electrostatic layer on the negatively charged pre-adsorbed BOD layer. The PEI/BOD/C modified electrode was regarded as one layer of multilayer films modified carbon electrode (step one). The additional layers of multilayer films modified carbon electrode were assembled by repeating the process of step 1 ($n$−1) times. This method of enzyme immobilization forms large three-dimensional multilayer structures of BOD–PEI complexes which promotes the preservation of the catalytic activity of immobilized BOD in solution and in the dehydrated state.

#### 2.2.2. Coimmobilization of BOD and carbon nanotubes by encapsulation into a Nafion film

To prepare an ink of carbon nanotubes we have used commercially available SWNTs. The SWNTs were dispersed in deionized water at a final concentration of approximately 1 mg/ml. 0.1 ml of CNT suspension were mixed with 2 mg BOD and sonicated for 5 min to give stable BOD/CNT suspensions. BOD molecules were physically adsorbed onto the surface of CNT during mixing to develop homogeneous BOD/CNT ink (Fig. 1). 5 µl of BOD/CNT suspension were spread on carbon electrode surface and allowed to dry at ambient temperature for 60 min. Then 3 µl of 0.5% Tetrabutylammonium bromide salt-treated Nafion solution [64] were spread on the BOD/CNT/C electrode surface and allowed to evaporate in air for 10 min. The electrode was rinsed three times with water and soaked for at least 30 min in 0.1 M phosphate buffer (pH 7.0) before use. The mixture-casting of Nafion modified with quaternary ammonium bromides increases the size of the pore structure and decreases pore density [64]. The proton exchange Nafion membrane acts as an insoluble solid polymer electrolyte and was used as a binder to hold the BOD/CNT on the electrode surface (Fig. 1d).

### 2.3. The Angle Resolved X-ray photoelectron spectroscopy

ARXPS spectra were acquired by a Kratos AXIS Ultra photoelectron spectrometer using a monochromatic Al Kα source operating at 300 W. The base pressure was $2\times10^{-10}$ Torr, and operating pressure was $2\times10^{-9}$ Torr. Charge compensation was accomplished using low energy electrons. Standard operating conditions for good charge compensation are −4.1 V bias voltage, −1.0 V filament voltage and a filament current of 2.1 A. The BOD samples with 1, 2 and 3 layers that have been assembled by a layer-by-layer approach are referred as 1L, 2L and 3L through the manuscript. To eliminate contribution of the underlying substrate into ARXPS sampling depth, reference spectra for BOD and PEI were obtained from thick films (>5 µm) created by solvent casting 0.2% solutions of BOD and PEI onto a glass slide. In addition, a carbon electrode itself (CE), a carbon electrode activated by GA (CE+GA) and a carbon electrode with individual layers of BOD (CE+BOD) and PEI (CE+PEI) were analyzed as well. The reported ARXPS data represent averages from 2–3 areas per sample on two different samples. The survey of each area is done first, followed by the recording of high-resolution spectra of C 1s, O 1s and N 1s for all the samples. The following take-off angles (TOA) are selected for angle resolved studies (Fig. 2): 90°, 50°, 35°, 25° and 15°. In ARXPS, changing the angle of the sample with respect to the direction probed by the detector, the so-called take-off-

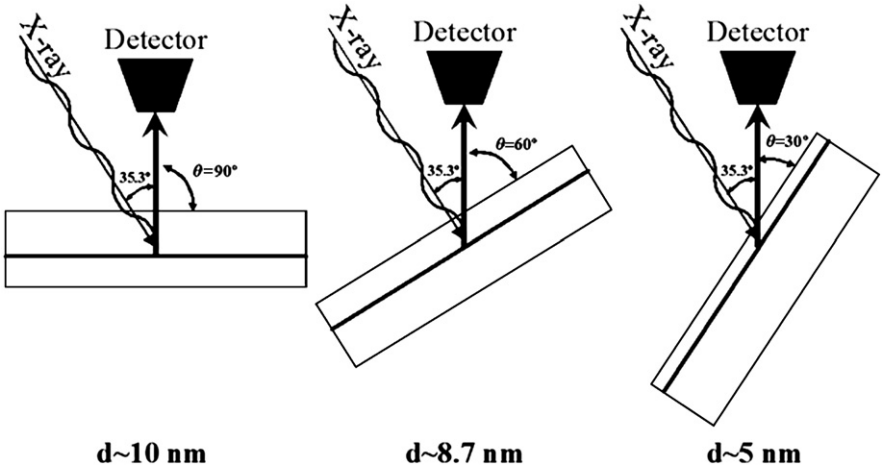


**Fig. 2.** The principle of Angle Resolved XPS analysis. By tilting the sample with respect to the detector the sampling depth decreases from approximately 10 nm for 90° to approximately 5 nm at 30°.

angles, one can vary the effective sampling depth. The approximate depth sampled, $d$, is given by the equation:

$$d = 3\lambda \sin\theta, \quad (1)$$

where $\lambda$ is the inelastic mean free path of the photoelectron and $\theta$ is the angle between the sample surface and the detector acceptance direction. Thus at $\theta$=90° the sample surface is perpendicular to the line of acceptance of the analyzer, and $d$ is the maximum sampling depth of $3\lambda$. As $\theta$ is reduced then the sampling depth decreases as seen in Fig. 2.

Linear background was used for elemental quantification of C 1s, N 1s and O 1s spectra. Quantification utilized sensitivity factors provided by the manufacturer. All the spectra were charge referenced to the aliphatic carbon at 284.8 eV. Curve fitting was carried out using individual peaks of constrained width, position and 70% Gaussian/30% Lorentzian line shape. Relative thicknesses of individual layers were calculated by using substrate/overlayer model in Arctick [50].

### 2.4. Electrochemistry

Cyclic voltammetry (CV) was performed on an EG&G potentiostat-galvanostat (model 263A). The BOD modified and unmodified carbon electrodes were used as indicator and counter electrodes, respectively. The reference electrode was Ag/AgCl. In all experiments a one-compartment electrochemical cell (volume 4 mL) was used. The CVs of BOD electrodes were measured in the absence (under anaerobic conditions) and in the presence (aerobic conditions) of oxygen with a potential scan from negative to positive potential and back to the original negative potential by changing the applied potential from −0.2 V to 0.8 V vs. Ag/AgCl. At the start of the experiments nitrogen or oxygen was bubbled through the buffer solution for 40 min. All electrochemical experiments were carried out at 20±0.5 °C. Data of cyclic voltammetry were used to calculate the electron-transfer rate constant using the method of Laviron [51]. The saturating concentration of oxygen was 1.2 mM. 1,4-hydroquinone, bilirubin and ABTS were used as models for studying the kinetics and mechanism of mediated electron transfer. The electrode potentials are given versus Ag/AgCl, 3M KCl reference electrode.

#### 2.4.1. Determination of BOD surface concentration

The surface coverage by BOD was determined by measuring the Faradic charge ($Q$) using slow scan rate voltammetry, according to [29]:

$$\Gamma = Q/nFA \quad (2)$$

where $\Gamma$ is the surface concentration of BOD, $Q$ is the charge obtained from integration of the anodic peak, $n$ is the number of electrons per oxidation of BOD molecule, $F$ is the Faraday constant, and $A$ is the electrode surface area in contact with the electrolyte. This surface area was calculated using the capacitance of the electrode obtained from cyclic voltammetry in a potential region where no Faradic processes occur. In order to elucidate the surface area the specific capacitance for carbon material was determined to be 20 μF/cm$^2$. The capacitance of carbon electrodes has been determined by using Mott–Schottky plots at fixed frequency [65–67]. To measure the impedance, a software EIS 300 and Reference 600 Potentiostat/Galvanostat/ZRA from Gamry Instruments Co have been used. Electrochemical impedance was measured by applying an AC potential to an electrochemical cell and measuring the current through the cell. The response to this potential is an AC current signal that was analyzed as a sum of sinusoidal functions (a Fourier series).

## 3. Results and discussions

### 3.1. Studying the physical architecture of ultrathin PEI/BOD films on the electrode surface by ARXPS spectroscopy

The physical architecture of ultra thin BOD films, including elemental and chemical composition, layer-by-layer assembly and relative thickness of adsorbed layers, was investigated by Angle Resolved X-ray photoelectron spectroscopy [46–48].

Table 1 shows the elemental composition and deconvolution curve fit results for high-resolution C 1s spectra for 90° and 15° TOA for all samples.

As reference samples we have used an unmodified carbon electrode and thick films from pure BOD and PEI. No data for 15° TOA are shown for reference samples, as they are statistically the same as for 90°. The carbon electrode itself (CE) has 20% of oxygen and a variety of C–C and C–O species. Importantly, its composition does not change with depth indicating that there is no hydrocarbon or any other contamination at the surface and oxygen is a part of the electrode surface itself, rather than contamination. The carbon electrode surface, which has been preliminary activated by glutaraldehyde (CE+GA), does not show any changes in elemental composition, but shows an enrichment of unsaturated carbons and a slight enrichment in oxygen at the top surface of the electrode. This fact indicates adsorption of glutaraldehyde molecules on the carbon surface. A typical high-resolution C 1s spectrum of the unmodified carbon electrode, pure PEI and BOD, and 2L layer-by-layer samples are presented in Fig. 3.

Carbon from the electrode has a unique peak at 284.6 eV. A pure BOD has a unique peak at 288.5 eV in the C 1s high-resolution spectrum due to the presence of COOH/N–C═O types of species, while pure PEI has a single type of carbon detected due to C–NH at 285.5 eV (Table 1). Pure BOD has significant amounts of oxygen and 6% of nitrogen, while PEI has 28% of nitrogen and the rest (72%) is carbon.

ARXPS analysis of a PEI layer deposited on a carbon electrode surface (CE+PEI) shows a slight increase of nitrogen, while the distribution of C species almost does not change with depth. A unique peak at 287.5 eV is observed for CE+PEI sample, which might be the result of an interaction between amino groups of PEI and aldehyde groups at the carbon surface. Enrichment of this type of species at deeper depth compared to shallower depths confirms that this might be a representation of an interaction between the CE+GA and PEI. For a BOD layer deposited on carbon electrode surface (CE+BOD) a unique significant peak at 288.5 eV for BOD is observed, in addition to large

**Table 1**
XPS quantitative results

| | Elemental, % | | | C 1s deconvolution, % | | | | |
|---|---|---|---|---|---|---|---|---|
| | C 1s | O 1s | N 1s | 284.6 | 285.2 | 286.4 | 287.5 | 288.5 |
| | | | | C═C | C–C, C*–CO | C–N | C–O | N–C═O, COOH |
| BOD 90 | 63.3 | 30.9 | 5.9 | – | 23.8 | 25.3 | – | *14.2* |
| PEI 90 | 72.2 | – | *27.8* | – | *72.2* | – | – | – |
| CE 90 | 77.8 | 22.2 | – | 41.1 | 23.3 | 12.1 | – | 1.3 |
| CE+GA 90 | 77.8 | 22.2 | – | 48.6 | 12.0 | 14.9 | – | 2.3 |
| CE+GA 15 | 76.0 | 24.0 | – | 60.2 | 7.5 | 8.3 | – | – |
| CE+PEI 90 | 74.8 | 22.1 | 3.1 | 40.5 | 22.3 | 8.1 | 3.9 | – |
| CE+PEI 15 | 72.8 | 25.4 | 1.9 | 42.0 | 24.7 | 4.8 | 1.2 | – |
| CE+BOD 90 | 63.3 | 30.5 | 6.2 | 16.9 | 21.7 | 16.2 | – | 8.6 |
| CE+BOD 15 | 66.9 | 28.1 | 5.0 | 22.7 | 25.2 | 12.2 | – | 6.9 |
| 1L 90 | 72.6 | 25.9 | 1.5 | 41.6 | 20.0 | 5.0 | 0.0 | 6.0 |
| 1L 15 | 78.9 | 19.6 | 1.5 | 51.4 | 20.2 | 3.1 | 1.3 | 2.9 |
| 2L 90 | 66.4 | 30.1 | 3.5 | 32.0 | 18.7 | 8.4 | 1.5 | 5.8 |
| 2L 15 | 72.4 | 24.8 | 2.8 | 38.7 | 23.4 | 5.1 | 2.6 | 2.5 |
| 3L 90 | 74.4 | 20.7 | 5.0 | 44.3 | 18.0 | 7.9 | 1.5 | 2.8 |
| 3L 15 | 81.8 | 15.3 | 3.0 | 46.9 | 24.9 | 6.4 | 1.3 | 2.3 |

Elemental % and C 1s deconvolution.

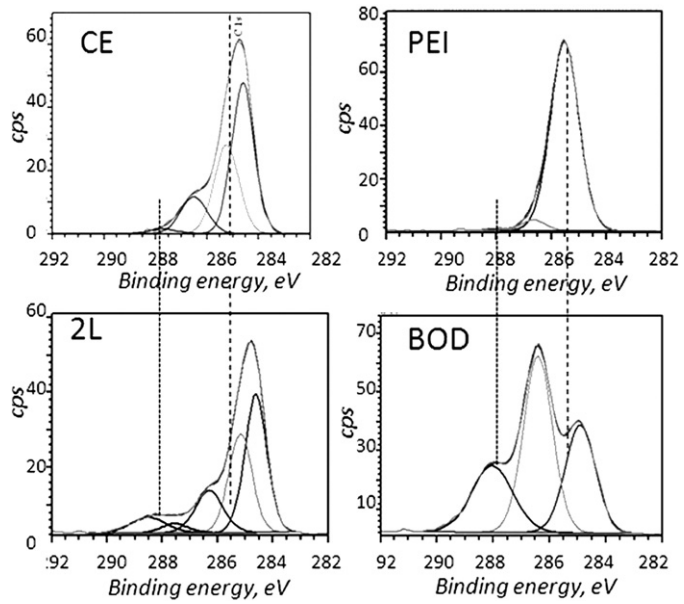


**Fig. 3.** XPS spectra of carbon electrode (CE), soluble pure polyethilenimine (PEI), soluble pure bilirubin oxidase (BOD) and BOD/PEI 2 bi-layered sample.

peak at 284.6 eV for CE. Each of the components of the layer-by-layer samples, thus, has a unique peak within C 1s XPS spectra which can be used to distinguish between individual layers on electrode surface. However, intermolecular interactions between polymer and an enzyme in layer-by-layer samples may slightly shift the position of these unique peaks.

For layer-by-layer samples (1L, 2L, 3L), an increase of the nitrogen percentage (%N) with an increase of number of bi-layers manifests the layer growth. The amount of %N in layered samples is much smaller than that for reference pure samples of PEI and BOD, indicative of ultrathin monolayer formation. High-resolution C 1s spectra for layer-by-layer samples have a substantial peak at 288.5 eV coming from BOD, which is larger for deeper sampling depths for all samples, confirming BOD as being a first deposited layer for all samples. This peak is decreased with increase of the number of BOD/PEI bi-layers. This decrease may be caused by expected attenuation of the signal from BOD by the top PEI layer, but also by a chemical shift of unique peak of BOD due to interaction between PEI and BOD. An increase of % N with the number of layers suggests that this decrease in the peak at 288.5 eV is mainly due to an increasing PEI contribution into the layer-by-layer samples.

All layer-by-layered samples have the same unique peak that is only present in CE+PEI sample, which we have attributed above to an interaction between the CE+GA and PEI mainly. Based on the above discussion, we assume that this interaction component dominates possible insignificant contribution from a chemical shift in peak at 288.5 eV due to an interaction between BOD and PEI. Existence of this peak, thus, for layer-by-layer samples, indicates non-uniform coverage of BOD on, a probably, really rough carbon electrode surface. It may indicate that part of the CE surface is coming in contact with the PEI layer, which interacts with aldehyde groups directly on the CE surface. Interestingly, for the 1L sample, this peak is absent at 90° TOA indicating that we only detect BOD on CE for this depth, and it contributes ~1.5% of N. The presence of this peak at shallower depths for the 1L sample confirms an ultrathin layer of PEI on top of BOD and, possibly, an interaction of PEI with the carbon electrode. This component is more significant for the 2L sample, while it diminishes for 3L, indicating that the entire CE is now being covered by the previously deposited BOD/PEI layers. Thus, ARXPS data confirm the formation of ultrathin layer-by-layer architectures, where BOD is the first and PEI is the second part of a bi-layered structure. Importantly, layers are not discrete, but rather some intermixing of layers occurs. Unique peaks of BOD at 288.5 eV and of CE at 284.6 eV were used in a substrate overlayer model for estimation of the relative thickness of the 1st layer of BOD on the carbon electrode surface. At the same time, there is a challenge to estimate the PEI thickness on BOD using the same approach. Even though PEI has a unique peak at 285.4 eV, both BOD and CE also contribute to this part of the C 1s spectrum. The peak at 287.5 eV, being a unique peak due to an interaction component, may be used in attempt to get relative values of PEI thickness on BOD. The values of thicknesses of BOD and PEI obtained can only be used for relative comparison between samples. The thicknesses of layers calculated via the substrate/overlayer model using the 288.5 eV peak for BOD, the 284.6 eV peak for CE and the 287.5 eV peak for PEI are shown in Table 2.

The thickness of each individual BOD/PEI by-layer is on the same order of magnitude as a few macromolecular layers, i.e. in the nanometer range. The thickness of BOD on CE increases ~2-fold from 1 to 2-layered sample. However, the 3-layered sample does not show the expected increase in BOD thickness, most probably due to partial interpenetration of neighboring BOD and PEI layers. The reason of that is the BOD and PEI layers are not discrete, but rather some intermixing of layer occurs. The rough surface of the carbon electrode probably promotes a mixing of neighboring layers. Interestingly, the same is observed when relative thicknesses on PEI on BOD are calculated for the peak at 287.5 eV. Thus, the obtained architectures for 1L and 2L samples are ordered with some degree of intermixing and stable due to the strong electrostatic attraction between the successive polyion and protein layers, while for samples with more layers, a large degree of intermixing and loss of order is observed.

### *3.2. Direct electrochemistry of bilirubin oxidase at carbon electrode surface*

The electrochemical studies of PEI/BOD films (Fig. 4a) formed on the surface of a carbon electrode by layer-by-layer technique have demonstrated that only the first two layers of immobilized BOD are electroactive with sets of anodic and cathodic peaks corresponding to redox centers of BOD in the potential areas between 0 and 600 mV.

Considering that the electrochemically accessible surface area of the carbon electrode is 0.02 $cm^2$, the surface concentration of electroactive BOD in terms of DET is $3.2\times10^{-10}$ mol/$cm^2$, and the total amount of BOD immobilized on the electrode surface is $3.5\times10^{-8}$ mol/$cm^2$, we have determined that only a negligible part (1%–2%) of the immobilized BOD molecules (as a first monolayer on the electrode surface) participates in direct electrical communication with the electrode. This means that mediatorless electrical communication between the redox centers of BOD and the electrode takes place mainly through a direct physical contact of enzyme molecules with the electrode surface. A similar conclusion was made by Lim et al. [62]. The ARXPS data have shown that the BOD and PEI layers adsorbed on the electrode surface are not discrete, but rather some intermixing of layer occurs. A partial interpenetration of neighboring BOD and PEI layers probably facilitates electron-transfer communication between redox copper centers of the enzyme and electrode surface because PEI has a high binding affinity towards a negatively charged carbon surface and BOD molecules and a high electron-donating capability [29,49,52–54]. According to [52–54], the electron-donating ability of PEI mainly depends on the number of amino groups adsorbed on the electrode surface. About 25% of the

**Table 2**
Overall relative thickness of BOD and PEI layers determined from overlayer model

| | BOD thickness on CE, *nm* | PEI thickness on BOD, 287.5, *nm* |
|---|---|---|
| L1 | 0.13 | 0.26 |
| L2 | 0.30 | 0.74 |
| L3 | 0.21 | 0.35 |

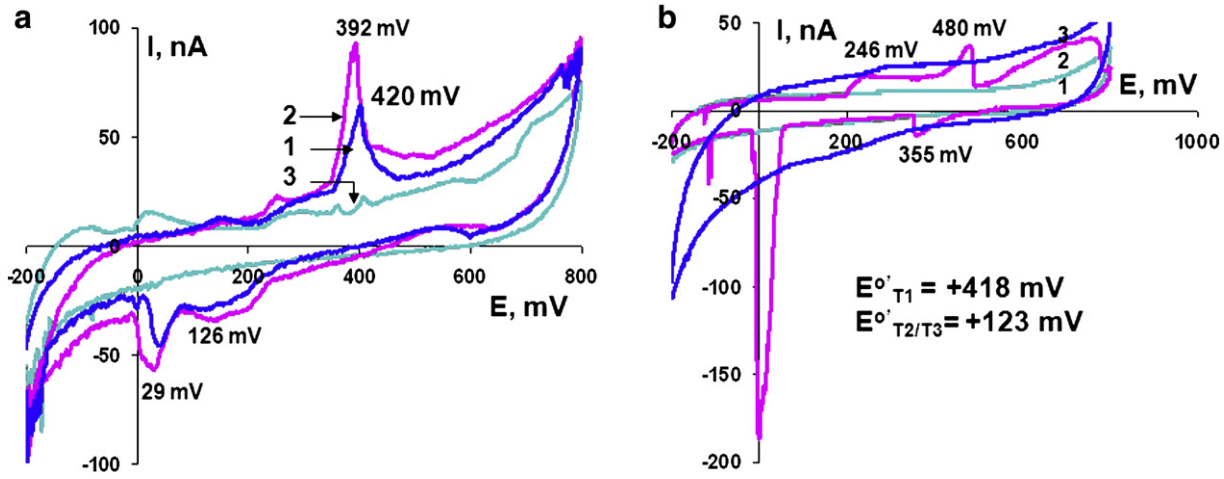


**Fig. 4.** a. Cyclic voltammograms of bilirubin oxidase from the fungi *Myrothecium verrucaria* immobilized on carbon electrode in 0.1 M acetate buffer (pH 4.9) under anaerobic conditions. The number of BOD/PEI layers increases from 1 to 3. b. Cyclic voltammograms of *Myrothecium verrucaria* bilirubin oxidase immobilized on the carbon electrode in 0.1 M acetate buffer (pH 4.9) under anaerobic (2) and aerobic (3) conditions. 1 — PEI/C electrode; 2 — and 3 — PEI/BOD/C electrodes; scan rate 10 mV/s.

amino groups of PEI are primary and about 50% are secondary, and each amino group contributes 0.04 electrons [54]. Considering all these facts together, we suppose that one of the possible ways of intramolecular electron transfer might be electron flow from redox centers of BOD to the electrode surface through the amino groups of PEI and protein molecules adsorbed directly on the electrode surface.

Fig. 4b curve 2 presents a voltammorgam of a BOD-modified electrode with two distinct redox peaks corresponding to reduction and oxidation of the first and second redox centers of BOD in anaerobic and aerobic conditions. We assume that the formal potential of +418 mV vs. Ag/AgCl belongs to T1 copper center of BOD. This value of redox potential is in good agreement with data obtained by other authors for the T1 copper center of BOD [14,19,22,24,25]. The anodic and cathodic peaks corresponding to the T1 copper center are clearly observed at pH 4.9 (Fig. 4b curve 2), but less distinct at neutral pH (Fig. 5a). Since the redox centers of BOD occupy only a small part of the enzyme macromolecule, the increasing pH of the solution may affect the bond lengths between the coordinating copper atoms and histidine residues and the architecture of other ligand groups [55]. As a result, the kinetics of electrical communication between the T1 copper centers and the electrode is slowing down, and anodic and cathodic current peaks become less defined. Interestingly, an analogous tendency, i.e. weakening of signal intensity related to the T1 copper center, has been also observed by authors [17] during studies of pH dependencies of electron paramagnetic resonance (EPR) spectra of BOD. Both the T1 and T2 copper signals were fully observed at pH 5.3, but signal intensity of the T1 copper became weaker with an increase of solution pH. The CV of BOD film in potential area between 0.0 V and 0.3 V (Fig. 4b) has strongly asymmetric anodic and cathodic peak shapes. The reduction peak current was significantly higher then the oxidation. Since bilirubin oxidase is a multicenter enzyme, intermediate redox states are expected [11]. Therefore, we assume that the pair of redox anodic and cathodic peaks in potential area between 0.0 V and 0.3 V belongs probably to the process of direct electrical communication between the T2/T3 redox copper center of BOD and the electrode (Fig. 4b curve 2). By using Laviron plot [51], we have calculated electron-transfer rate constant for BOD. It is 1.5 $s^{-1}$, which is close to ET rate constant of laccase [49].

That BOD can undergo non-catalytic direct electron transfer between enzyme and electrode and retain its catalytic activity has been confirmed by the study of bioelectrocatalytic activity of BOD on the electrode surface in the presence of oxygen only and in the presence of both oxygen and ABTS as a redox mediator (Figs. 4b, 5a, and 6b). As seen in Fig. 4b

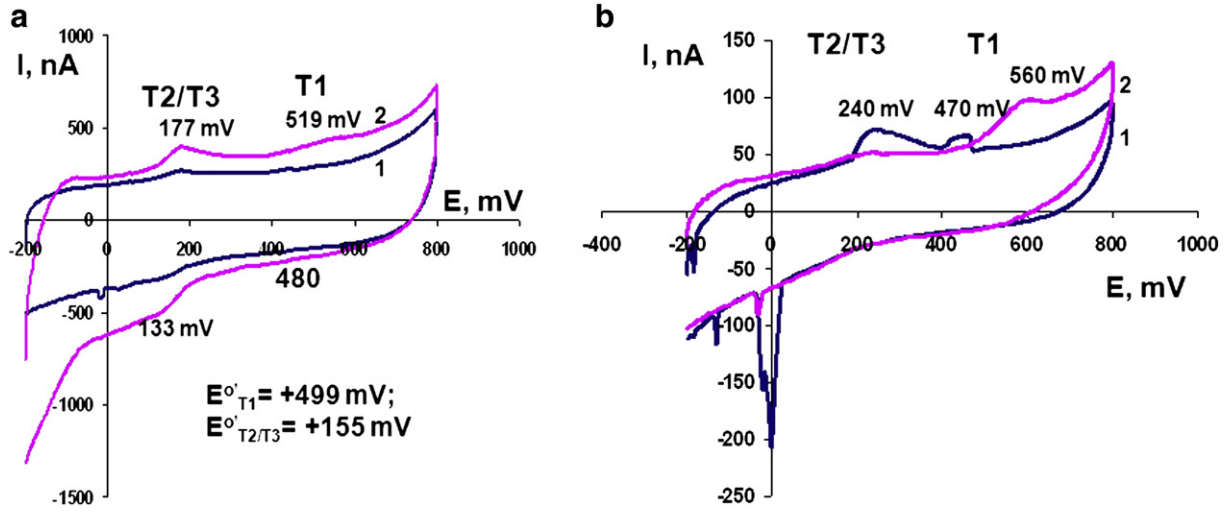


**Fig. 5.** a. Cyclic voltammograms of the PEI/BOD/C electrode in 0.1 M phosphate buffer, (pH 6.8) under anaerobic (1) and aerobic (2) conditions. Scan rate 10 mV/s. b. Cyclic voltammograms of the PEI/BOD/C electrode in 0.1 M acetate buffer, (pH 4.9) under anaerobic conditions. 1 — in the absence and 2 — in the presence of 2.0 mM bathocuproine disulfonate; scan rate 10 mV/s.

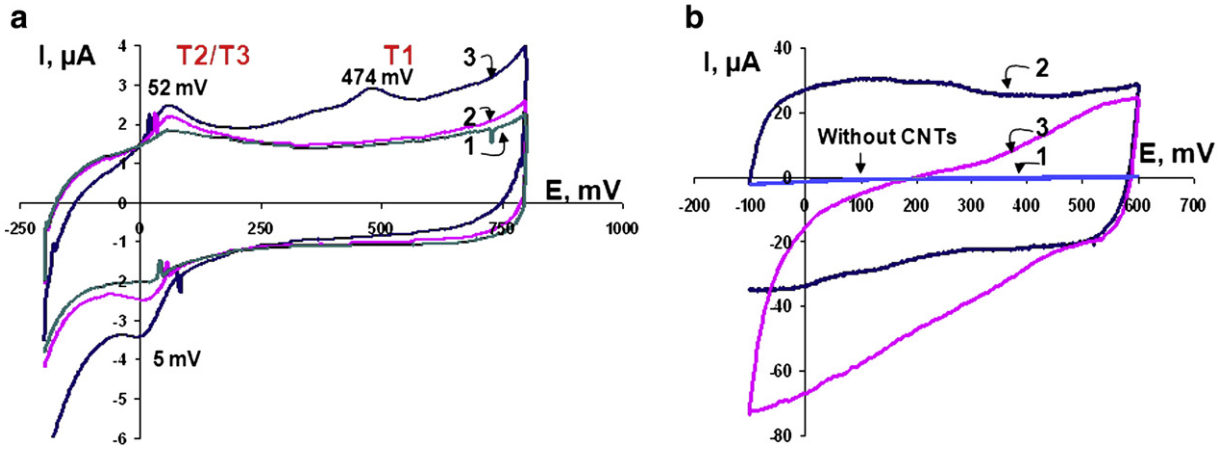


**Fig. 6.** a. Cyclic voltammograms of the Nafion/BOD/SWNTs/C modified electrode in 0.1 M phosphate buffer, (pH 6.8) under aerobic conditions. Bilirubin: 1 — 0; 2 — 5 μM; 3 — 40 μM; Scan rate: 20 mV/s. b. Cyclic voltammograms of the Nafion/BOD/SWNTs/TP modified electrode in 0.1 M phosphate buffer, (pH 6.8) under anaerobic (2) and aerobic (3) conditions. 1 — TP; 2 — and 3 — Nafion/BOD/SWNTs/TP.

curve 1, the process of a non-catalytic oxygen reduction on a carbon electrode in the absence of BOD is beginning at a potential lower than −150 mV vs. Ag/AgCl. However, in the presence of bilirubin oxidase the bioelectrocatalytic process of oxygen reduction starts at a much more positive potential (+460 mV), which is close to the redox potential of T1 copper centers of BOD. This fact indicates that the T1 copper center is the primary electron acceptor from the electron donor substrate followed by electron transfer to the trinuclear T2/T3 copper center [11,14,25,26]. In the presence of oxygen, anodic and cathodic peaks are transformed to catalytic sigmoidal waves (Figs. 4b curve3 and 5a curve 2). The half-wave potential of oxygen reduction ($E$=+155 mV) is comparable to the values obtained by authors [14,25] at pyrolytic and spectrographic graphites. Thus, the potential area between 0.0 V and +0.4 V can be considered related to the oxygen-reducing site of the T2/T3 copper center. This is also supported by voltammograms in the presence of bathocuproine disulfonate (BCS) in anaerobic conditions (Fig. 5b).

The BCS is a chelating agent that creates strong and specific cuprous-bathocuproine sulfonate complex $(BCS)_2Cu(I)$ exclusively with the T2 copper ion located in trinuclear redox copper center of multicopper oxidases [56,57]. The BCS is widely used also for quantitative determination of Cu(I) in different samples [58]. As shown in Fig. 5b curve 2, in the presence of BCS in 0.1 M phosphate buffer solution, pH 6.8, the anodic and cathodic peaks in potential areas related to the T2/T3 copper center (from −50 mV to 400 mV vs. Ag/AgCl) have completely disappeared. At the same time, the anodic peak related to the T1 copper center (potential area between 0.4 V and 0.6 V) just has shifted to the more positive potential area from +450 mV to +560 mV and a current of the peak is increased in more than three times (Fig. 5b curve 2). Electron paramagnetic resonance analysis of the native and copper-depleted fungal laccase [56,57] has shown that BCS chelating agent creates strong and very specific complex with T2 copper ion of trinuclear copper center of laccase. As a result of that, the T2 copper ion is completely removed from a redox copper center of enzyme. The spectral characteristics of the copper-depleted enzyme indicate that T1 copper center appears unchanged [56]. Based on EPR and resonance Raman spectroscopy [59], it was concluded that the removal of T2 copper as a result of complex formation $(BCS)_2Cu(I)$ is accompanied by structural changes of the enzyme that affect the type-1 copper site. In fact, the analogous events we have seen for bilirubin oxidase in the presence of BCS (Fig. 5b) are: a) disappearance of the anodic and cathodic peaks related to the T2/T3 copper center in potential areas between −50 mV and 400 mV and b) changes in position of the anodic peak of the T1 copper center from +470 mV to +560 mV probably as a result of structural changes of BOD. Thus, the electrochemical analysis of the redox copper centers of BOD by using bathocuproine disulfonate as a specific chelating agent for the T2 copper center has confirmed that the potential area between 0.0 V and +0.4 V belongs to the oxygen-reducing site of the trinuclear copper center of the enzyme.

A significant breakthrough in the area of DET has been achieved by using carbon nanotubes (CNTs) as promoters of direct bioelectrocatalysis [8,41–45,60–62]. They are excellent conducting "nanowires" between the redox centers of an enzyme and the electrode surface. The assembly of SWNT/protein films provides a general way towards a design of nanostructured bio-functional surfaces in a highly controllable and robust manner [41–45]. Here, we have investigated the electrochemical behavior of BOD encapsulated in nanostructured carbon nanotube/Nafion composite electrodes. An electrical contact between the redox center of BOD and the carbon electrode is provided through the single-walled carbon nanotubes located on the electrode surface (Fig. 1). Fig. 6a shows the cyclic voltammograms of a Nafion/BOD/SWNTs/C modified electrode in 0.1 M phosphate buffer (pH 6.8) in aerobic conditions. The pair of nearly symmetric redox anodic and cathodic peaks related to the process of direct electrical communication between the T2/T3 redox copper center of BOD and the electrode was observed in potential area between 0.0 V and 0.1 V (Fig. 6a curve 1). However, the anodic and cathodic redox peaks related to the T1 copper center are not observed in both anaerobic and aerobic conditions. Interesting data have been obtained in the presence of different concentrations of bilirubin (Fig. 6a). The $\Delta I_p$ in potential area between 0.0 V and 0.1 V increased with increasing concentration of bilirubin. The anodic peak ($E$=+474 mV) related to the process of the electron exchange between the electrode and the electroactive T1 redox copper center of BOD appeared in the presence of 40 μM bilirubin and higher in 0.1 M phosphate buffer (pH 6.8) (Fig. 6a curve 3).

This value is close to the potential of the anodic peak (+420 mV) obtained with PEI/BOD/C modified electrode.

In order to increase the amount of SWNTs on the electrode surface, we have used Toray carbon paper (TP) as a matrix with a highly porous three-dimensional network. The tetrabutylammonium bromide salt-treated Nafion have been used as a SWNTs and BOD binder [64]. The study of the bioelectrocatalytic activity of Nafion/BOD/SWNTs/TP electrodes in aerobic conditions has shown that the process of oxygen reduction starts at +460 mV vs. Ag/AgCl (Fig. 6b curve 3). It agrees well with the data reported by other authors [24,60–62]. This onset potential is 60 mV more positive in comparison to that of the oxygen reduction for the PEI/BOD/C electrode. The incorporation of the ink of BOD/SWNTs into the pores of TP results in a highly porous three-dimensional network with dramatically increased electrode surface area (two orders of magnitude) and provides efficient oxygen reduction at the electrode

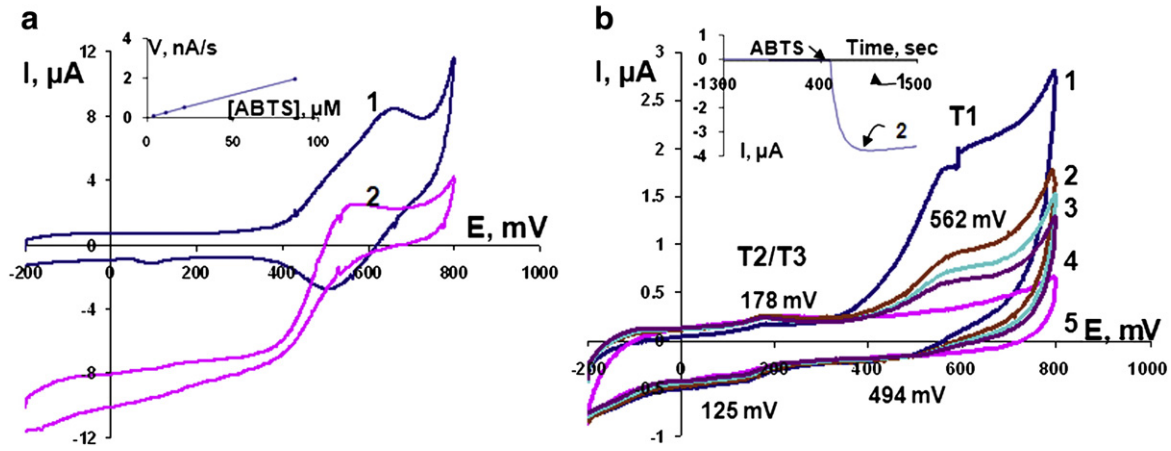


**Fig. 7.** a. Cyclic voltammograms of 0.18 mM ABTS in 0.1 M phosphate buffer, (pH 6.8) under aerobic conditions. 1 — PEI/C electrode; 2 — PEI/BOD/C electrode; scan rate 20 mV/s. Inset: calibration curve for ABTS using PEI/BOD/C electrode. The measurements were conducted in 0.1 M phosphate buffer, (pH 6.8). Applied potential is 0.0 V vs. Ag/AgCl; b. Cyclic voltammograms of PEI/BOD/C electrode in 0.1 M phosphate buffer, (pH 6.8) under aerobic conditions. Scan rate 10 mV/s. 1 — after BOD inactivation by 80 μM ABTS; 2–4 CVs of the same electrode in fresh buffer after washing steps; 5 — BOD active. Inset: amperometric responses of PEI/BOD/C electrode; 1-enzyme inactivated; 2-after enzyme reactivation; applied potential is 0.0 V vs. Ag/AgCl.

surface. Double layer capacitance of the SWNT-modified carbon electrode is substantially higher from that of the blank (unmodified) carbon electrode (Fig. 6b, curves 1 and 2). This attests to the substantial increase in the electrochemically accessible surface are of the SWNT-modified electrode.

In separate experiments we have investigated the catalytic activity of BOD in the presence of redox mediators (ABTS and 1,4-hydroquinone (HQ)). Fig. 7a shows the voltammograms of 0.18 mM ABTS at the PEI/C and BOD/PEI/C electrode in aerobic conditions. As demonstrated in Fig. 7a curve 2, the BOD/PEI/C modified electrode shows a good catalytic current toward oxygen reduction in a 20 mM phosphate buffer solution (pH 6.8) containing 0.18 mM ABTS as an electron-transfer mediator. The biocatalytic process of oxygen reduction in the presence of ABTS has started at a potential of +550 mV (Fig. 7a curve 2). The onset of non-biocatalytic oxygen reduction was observed at around −150 mV (Fig. 4b, curve 1). It indicates that soluble ABTS molecules, as an electron relay, markedly shifted the onset potential to a more positive potential area (+550 mV) and enhanced the electrocatalytic cathodic current significantly. However, we found that as a result of consecutive injections of gradually increasing concentrations of ABTS in 0.1 M phosphate buffer (pH 6.8), the rate of electron transfer and catalytic activity of immobilized BOD drastically decreased (Fig. 7b, inset). In fact, the current response of the BOD-modified electrode in the presence of 80 μM ABTS approached zero (Fig. 7b, inset curve 1). Instability and fast deactivation of the enzyme in the presence of ABTS was also reported by other authors [63]. We have established that the process of inactivation and reactivation of BOD by ABTS is reversible (Fig. 7b, inset curve 2). After washing the electrode several times, the shape of the voltammograms of BOD are completely restored (Fig. 7b curves 2–5). It is interesting to note that the shape of the voltammogram of inactivated BOD (Fig. 7b curve 1) is not the same as the one in the case of inactivated laccase [49]. Anodic current peaks of laccase inactivated by 1,4-hydroquinone are increased up to a factor of 8 in potential areas related to both T2/T3 and T1 redox copper centers simultaneously [49]. In the case of BOD inactivated by a high concentration of ABTS, the anodic current peak is increased in the potential area related to the T1 copper center only (Fig. 7b curve 1). It is important also to underline that unlike laccase, bilirubin oxidase is not inhibited by 1,4-hydroquinone in buffer solution (data not shown). Using an Eadie–Hofstee plot, we have calculated that the apparent $K_m$ and $V_{max}$ for BOD for 1,4-hydroquinone in 0.1 M phosphate buffer (pH 6.8) is 0.91 mM and 51.6 nA/s, consequently. This indicates that the affinity of the BOD redox copper center to hydroquinone is much lower than in the case of laccase [49].

## 4. Conclusions

This paper, for the first time, demonstrates important capabilities of Angle Resolved X-ray photoelectron spectroscopy for detailed analysis of the physical architecture of ultra thin layer-by-layer deposited films. Unique peaks within C 1s XPS spectra for each component of layer-by-layer assemblies have been used to distinguish individual layers on the electrode surface between each other. Angle-resolved XPS was used to follow ultrathin layer-by-layer formation. The layers are not discrete, but rather some intermixing of layer occurs. The thickness of each individual BOD/PEI bi-layer determined through the overlayer model is of the same order of magnitude than a few macromolecular layers, i.e. in the nanometer range.

The electrochemical studies of PEI/BOD films have demonstrated that mediatorless electrical communication between the redox centers of BOD and the electrode took place mainly through a direct physical contact of enzyme molecules with an electrode surface. The analysis of the redox copper centers of BOD in the presence of a chelating agent specific for T2 copper center only has shown that a potential area between 0.0 V and +0.4 V belongs to the oxygen-reducing site of the trinuclear copper center of the enzyme. Obviously, in order to discriminate individual redox potentials of T2 and T3 redox centers from each other, additional studies with bathocuproine disulfonate reagent should be done. The nature of the microenvironment, pH, and the method of enzyme immobilization have contributed to the values and position of anodic and cathodic peaks of the T1 and T2/T3 redox centers of bilirubin oxidase. This is mainly due to non-covalent binding of copper ions in the active site of BOD and the fact that redox centers of BOD occupy only a small part of the enzyme molecule [11,19,55].

We assume that the mechanism of inactivation of BOD in the presence of ABTS seems to be the same as in case for laccase inactivation by hydroquinone molecules [49]. According to the accepted hopping intramolecular ET mechanism of oxygen reduction for BOD [11,14,18,20], the T1 is the primary mononuclear copper center which accepts electrons from ABTS, and then electrons shuttle to the T2/T3 redox copper center. The fully reduced trinuclear copper center reacts with dioxygen. However, at high concentration of ABTS part of ABTS molecules can probably reach the trinuclear T2/T3 copper center directly followed by electron transfer to the trinuclear cluster, thus avoiding a cysteine-histidine pathway. In this case the intramolecular hopping ET is switched to a non-hopping ET mechanism which blocks oxygen reduction.

We have demonstrated that SWNTs play an active role in DET between the active site of BOD and the electrode surface. The BOD/CNT/

C modified electrode provides an efficient electro-reduction of oxygen to water at a potential +460 mV vs. Ag/AgCl, which is close to the potential of the reversible $O_2/H_2O$ half-cell [16,22,37]. The combination of SWNTs with BOD provides an excellent opportunity for design and development of new generations of microscale membrane-less biofuel cells.

## Acknowledgements

This work was supported in part by a grant from DOD/AFOSR MURI Award Number: FA9550-06-1-0264, Fundamentals and Bioengineering of Enzymatic Fuel Cells and by the NSF I/URC membership support of Toyota Motor Engineering & Manufacturing North America (TEMA) and Toyota Motor Corporation. The authors also wish to thank Shelley Minteer (St. Louis University) for providing the tetrabutylammonium bromide modified Nafion.

## References

[1] A.L. Ghindilis, P. Atanasov, E. Wilkins, Enzyme catalyzed direct electron transfer: fundamentals and analytical applications, Electroanalysis 9 (1997) 661–674.
[2] I. Willner, B. Willner, E. Katz, Biomolecule-nanoparticle hybrid systems for bioelectronic applications, Bioelectrochemistry 70 (2007) 2–11.
[3] G.S. Sayler, M.L. Simpson, C.D. Cox, Emerging foundations: nano-engineering and bio-microelectronics for environmental biotechnology, Curr. Opin. Microbiol. 7 (2004) 267–273.
[4] K. Kano, T. Ikeda, Bioelectrocatalysis, powerful means of connecting electrochemistry to biochemistry and biotechnology, Electrochemistry 71 (2003) 86–99.
[5] S.C. Barton, J. Gallaway, P. Atanasov, Enzymatic biofuel cells for implantable and microscale devices, Chem. Rev. 104 (2004) 4867–4886.
[6] E. Katz, A.N. Shipway, I. Willner, Biochemical fuel cells, in: W. Vielstich, H.A. Gasteiger, A. Lamm (Eds.), Fuel Cells — Fundamentals and Survey of Systems, vol. 1, J. Wiley and Sons, Ltd, London, 2003, pp. 1–27, Ch. 21.
[7] Heller, Potentially implantable miniature batteries, Anal. Bioanal. Chem. 385 (2006) 469–473.
[8] D. Ivnitski, B. Branch, P. Atanasov, C. Apblett, Glucose oxidase anode for biofuel cell based on direct electron transfer, Electrochem. Commun. 8 (2006) 1204–1210.
[9] F. Davis, S.P.J. Higson, Biofuel cells — recent advances and applications, Biosens. Bioelectron. 22 (2007) 1224–1235.
[10] S.D. Minteer, B.Y. Liaw, M.J. Cooney, Enzyme-based biofuel cells, Curr. Opin. Biotechnol. 18 (2007) 228–234.
[11] E.I. Solomon, U.M. Sundaram, T.E. Machonkin, Multicopper oxidases and oxygenases, Chem. Rev. 96 (1996) 2563–2605.
[12] A. Shimizu, J.H. Kwon, T. Sasaki, T. Satoh, N. Sakurai, T. Sakurai, S. Yamaguchi, T. Samejima, *Myrothecium verrucaria* bilirubin oxidase and its mutants for potential copper ligands, Biochemistry 38 (1999) 3034–3042.
[13] N. Tanaka, S. Murao, Purification and some properties of bilirubin oxidase of *Myrothecium verrucaria* MT-1, Agr. Biol. Chem. 46 (1982) 2499–2503.
[14] S. Shleev, A.E. Kasmi, T. Ruzgas, L. Gorton, Direct heterogeneous electron transfer reactions of bilirubin oxidase at a spectrographic graphite electrode, Electrochem. Commun. 6 (2004) 934–939.
[15] S. Tsujimura, H. Tatsumi, J. Ogawa, S. Shimizu, K. Kano, T. Ikeda, Bioelectrocatalytic reduction of dioxygen to water at neutral pH using bilirubin oxidase as an enzyme and 2,2′-azinobis (3-ethylbenzothiazolin-6-sulfonate) as an electron transfer mediator, J. Electroanal. Chem. 496 (2001) 69–75.
[16] N. Mano, H.-H. Kim, A. Heller, On the relationship between the characteristics of bilirubin oxidases and $O_2$ cathodes based on their "wiring", J. Phys. Chem. B 106 (2002) 8842–8848.
[17] G. Zoppellaro, N. Sakurai, K. Kunishige, T. Sakurai, The reversible change in the redox state of T1 Cu in *Myrothecium verrucaria* bilirubin oxidase, Biosci. Biotechnol. Biochem. 68 (2004) 1998–2000.
[18] S. Shleev, J. Tkac, A. Christenson, T. Ruzgas, A.I. Yaropolov, J.W. Whittaker, Lo. Gorton, Direct electron transfer between copper-containing proteins and electrodes, Biosens. Bioelectron. 20 (2005) 2517–2554.
[19] F. Xu, W. Shin, S.H. Brown, J.A. Wahleithner, U.M. Sundaram, E.I. Solomon, A study of a series of recombinant fungal laccases and bilirubin oxidase that exhibit significant differences in redox potential, substrate specificity, and stability, Biochim. Biophys. Acta 1292 (1996) 303–311.
[20] S. Tsujimura, K. Kano, T. Ikeda, Bilirubin oxidase in multiple layers catalyzes four-electron reduction of dioxygen to water without redox mediators, J. Electroanal. Chem. 576 (2005) 113–120.
[21] T. Nakagawa, S. Tsujimura, K. Kano, T. Ikeda, Bilirubin oxidase and [Fe(CN)6]3-/4-modified electrode allowing diffusion-controlled reduction of $O_2$ to water at pH 7.0, Chem. Lett. 32 (2003) 54–55.
[22] A. Christenson, S. Shleev, N. Mano, A. Heller, L. Gorton, Redox potentials of the blue copper sites of bilirubin oxidases, Biochim. Biophys. Acta 1757 (2006) 1634–1641.
[23] M. Tominaga, M. Otani, M. Kishikawa, I. Taniguchi, UV-ozone treatments improved carbon black surface for direct electron-transfer reactions with bilirubin oxidase under aerobic conditions, Chem. Lett. 35 (2006) 1174–1175.
[24] M.C. Weigel, E. Tritscher, F. Lisdat, Direct electrochemical conversion of bilirubin oxidase at carbon nanotube-modified glassy carbon electrodes, Electrochem. Commun. 9 (2007) 689–693.
[25] S. Tsujimura, T. Nakagawa, K. Kano, T. Ikeda, Kinetic study of direct bioelectrocatalysis of dioxygen reduction with bilirubin oxidase at carbon electrodes, Electrochemistry 72 (2004) 437–439.
[26] E.I. Solomon, R.K. Szilagyi, S.D. George, L. Basumallick, Electronic structures of metal sites in proteins and models: contributions to function in blue copper proteins, Chem. Rev. 104 (2004) 419–458.
[27] T. Ikeda, K. Kano, An electrochemical approach to the studies of biological redox reactions and their applications to biosensors, bioreactors, and biofuel cells, J. Biosci. Bioeng. 92 (2001) 9–18.
[28] S. Tsujimura, A. Kuriyama, N. Fujieda, K. Kano, T. Ikeda, Mediated spectroelectrochemical titration of proteins for redox potential measurements by a separatorless one-compartment bulk electrolysis method, Anal. Biochem. 337 (2005) 325–331.
[29] J.F. Rusling, R.J. Forster, Electrochemical catalysis with redox polymer and polyion-protein films, J. Col. Intreface Sci, 262 (2003) 1–15.
[30] F.A. Armstrong, Insights from protein film voltammetry into mechanism of complex biological electron-transfer reactions, J. Chem. Soc., Dalton Trans. (2002) 661–671.
[31] C. Leger, S.J. Elliott, K.R. Hoke, L.J.C. Jeuken, A.K. Jones, F.A. Armstrong, Enzyme electrokinetics: Using protein film voltammetry to investigate redox enzymes and their mechanisms, Biochemistry 42 (2003) 8653.
[32] F.A. Armstrong, Recent developments in dynamic electrochemical studies of adsorbed enzymes and their active sites, Curr. Opin. Chem. Biology 9 (2005) 110–117.
[33] J. Hirst, Elucidating the mechanisms of coupled electron transfer and catalytic reactions by protein film voltammetry, Biochim. Biophys. Acta 1757 (2006) 225–239.
[34] Y. Lvov, K. Ariga, I. Ichinose, T. Kunitake, Assembly of multicomponent protein films by means of electrostatic layer-by-layer adsorption, J. Am. Chem. Soc. 117 (1995) 6117–6123.
[35] L. Zhao, H. Liu, N. Hu, Assembly of layer-by-layer films of heme proteins and single-walled carbon nanotubes: electrochemistry and electrocatalysis, Anal Bioanal. Chem. 384 (2006) 414–422.
[36] F.N. Crespilho, V. Zucolotto, J.O.N. Oliveira, F.C. Nart, Electrochemistry of layer-by-layer films, Int. J. Electrochem. Sci. 1 (2006) 194–214.
[37] C. Kang, H. Shin, A. Heller, On the stability of the "wired" bilirubin oxidase oxygen cathode in serum, Bioelectrochemistry 68 (68) (2006) 22–26.
[38] I. Willner, E. Katz, A.F. Buckmann, Self-powered enzyme-based biosensors, J. Am. Chem. Soc. 123 (2001) 10752–10753.
[39] D. Ivnitski, E. Wilkins, H.T. Tien, A. Ottova, Electrochemical biosensor based on supported planar lipid bilayers for fast detection of pathogenic bacteria, Electrochem. Commun. 2 (2000) 457–460.
[40] T. Wink, S.J. Zuilen, A. Bult, W.P. Bennekom, Self-assembled monolayers for biosensors, Analyst 122 (1997) 43R–50R.
[41] A. Guiseppi-Elie, C. Lei, R.H. Baughman, Direct electron transfer of glucose oxidase on carbon nanotubes, Nanotechnology 13 (2002) 559–564.
[42] C. Cai, J. Chen, Direct electron transfer of glucose oxidase promoted by carbon nanotubes, Anal. Biochem. 332 (2004) 75–83.
[43] J. Li, A. Cassell, L. Delzeit, J. Han, M. Meyyappan, Novel three-dimensional electrodes: electrochemical properties of carbon nanotube ensembles, J. Phys. Chem. B 106 (2002) 9299–9305.
[44] M. Musameh, J. Wang, A. Merkoci, Y. Lin, Low-potential stable NADH detection at carbon-nanotube-modified glassy carbon electrodes, Electrochem. Commun. 4 (2003) 743–746.
[45] J. Wang, G. Liu, M.R. Jan, Ultrasensitive electrical biosensing of proteins and DNA: carbon nanotube derived amplification of the recognition and transduction events, J. Am. Chem. Soc. 126 (2004) 3010–3011.
[46] P.J. Cumpson, in: D. Briggs, J.T. Grant (Eds.), Surface Analysis by Auger and X-ray Photoelectron Spectroscopy, IM publications and Surface Spectra Limited, Chichester: Manchester, 2003, Chapter Angle-Resolved X-Ray Photoelectron Spectroscopy.
[47] K.E. Nelson, L. Gamble, L.S. Jung, M.S. Boeckl, E. Naeemi, S.L. Golledge, T. Sasaki, D.G. Castner, C.T. Campbell, P.S. Stayton, Surface characterization of mixed self-assembled monolayers designed for streptavidin immobilization, Langmuir 17 (2001) 2807–2816.
[48] K. Artyushkova, J.E. Fulghum, Y. Reznikov, Orientation of 5CB molecules on aligning substrates studied by angle resolved X-ray photoelectron spectroscopy, Mol. Cryst. Liq. Cryst. 438 (2005) 1769–1777.
[49] D. Ivnitski, P. Atanassov, Electrochemical studies of intramolecular electron transfer in laccase from *Trametes versicolor*, Electroanalysis 19 (2007) 2307–2313.
[50] http://www.npl.co.uk/server.php?show=ConWebDoc.607.
[51] E. Laviron, General expression of the linear potential sweep voltammogram in the case of diffusionless electrochemical systems, J. Electroanal. Chem. 101 (1979) 19–28.
[52] A. Pardo, R. Basseguy, A. Bergel, Simple design of cast myoglobin/polyethyleneimine modified electrodes, J. Appl. Electrochem. 36 (2006) 835–842.
[53] M. Shim, A. Javey, N.W.S. Kam, H. Dai, Polymer functionalization for air-stable n-type carbon nanotube field-effect transistors, J. Am. Chem. Soc. 123 (2001) 11512–11513.
[54] K. Bradley, M. Briman, A. Star, G. Gruner, Charge transfer from adsorbed proteins, Nano. Lett. 4 (2004) 253–256.
[55] O. Farver, I. Pecht, Electron transfer in proteins: in search of preferential pathways, FASEB J. 5 (1991) 2554–2559.
[56] R. Malkin, B.G. Malmström, T. Vänngard, The reversible removal of one specific copper(I1) from fungal laccase, Eur. J. Biochem. 7 (1969) 253–259.
[57] O.V. Koroleva, E.V. Stepanova, V.P. Gavrilova, V.I. Biniukov, A.M. Pronin, Comparative characterization of methods for removal of Cu(II) from the active sites of fungal laccases, Biochemistry (Moscow) 66 (2001) 960–966.
[58] S. Mandal, N.H. Kazmi, L.M. Sayre, Ligand dependence in the copper-catalyzed oxidation of hydroquinones, Arch. Biochem. Biophys. 435 (2005) 21–31.
[59] T. Sakurai, S. Suzuki, Spectroscopy of cucumber ascorbate oxidase and fungal laccase, in: A. Messerschmidt (Ed.), Multi-Copper Oxidases, World Scientific, Singapore, 1997, pp. 225–250.

[60] W. Zheng, Q. Li, L. Su, Y. Yan, J. Zhang, L. Mao, Direct electrochemistry of multi-copper oxidases at carbon nanotubes noncovalently functionalized with cellulose derivatives, Electroanalysis 18 (2006) 587–594.
[61] J. Lim, P. Malati, F. Bonet, B. Dunn, Nanostructured sol–gel electrodes for biofuel cells, J. Electrochem. Soc. 154 (2007) A140–A145.
[62] J. Lim, N. Cirigliano, J. Wang, B. Dunn, Direct electron transfer in nanostructured sol–gel electrodes containing bilirubin oxidase, Phys. Chem. Chem. Phys. 9 (2007) 1–6.
[63] D. Quan, Y. Kim, W. Shin, Characterization of an amperometric laccase electrode covalently immobilized on platinum surface, J. Electroanal. Chem. 561 (2004) 181–189.
[64] N.L. Akers, C.M. Moore, S.D. Minteer, Development of alcohol/$O_2$ biofuel cells using salt-extraxted tetrabutylammonium bromide/Nafion membranes to immobilize Dehydrogenase enzymes, Electrochim. Acta 50 (2005) 2521–2525.
[65] E. Barsoukov, J.R. Macdonald, Impedance Spectroscopy: Theory, Experiment, and Applications, Wiley Interscience Publications, 2005 616 pp.
[66] A.J. Bard, L.R. Faulkner, Electrochemical Methods: Fundamentals and Applications, John Wiley & Sons, Inc, 2000 856 pp.
[67] F. Fabregat-Santiago, G. Garcia-Belmonte, J. Bisquert, P. Bogdanoff, A. Zabanc, Mott–Schottky analysis of nanoporous semiconductor electrodes in dielectric state deposited on $SnO_2$ (F) conducting substrates, J. Electrochem. Soc. 150 (2003) E293–E298.